

# In situ STM study of underpotential deposition of bismuth on Au(1 1 0) in perchloric acid solution

Masanori Hara<sup>a</sup>, Yoshiki Nagahara<sup>a</sup>, Junji Inukai<sup>a,b</sup>, Soichiro Yoshimoto<sup>a</sup>, Kingo Itaya<sup>a,c,\*</sup>

<sup>a</sup> Department of Applied Chemistry, Graduate School of Engineering, Tohoku University, 6-6-04 Aoba, Sendai 980-8579, Japan

<sup>b</sup> NICHe, Tohoku University, 6-6-10 Aoba, Sendai 980-8579, Japan

<sup>c</sup> CREST, JST, 4-1-8 Kawaguchi, Saitama 332-0012, Japan

Received 3 November 2004; received in revised form 15 January 2005; accepted 17 January 2005

Available online 12 September 2005

## Abstract

The underpotential deposition (UPD) of Bi on Au(1 1 0) was investigated in HClO<sub>4</sub> solution using in situ scanning tunneling microscopy. The UPD of Bi occurred in three steps. A  $\begin{pmatrix} 3 & 0 \\ 1 & 1 \end{pmatrix}$  structure, in which Bi atoms formed dimers, was found for the first UPD adlayer. A (1 × 1) image was obtained by STM at the second UPD peak. For the third UPD peak, Bi atoms formed an incommensurate adlayer, and stripes of Bi were observed on terraces. After the third UPD, a structural reconstruction caused by adsorbed Bi was observed.  
© 2005 Published by Elsevier Ltd.

**Keywords:** Au(1 1 0); Bi; UPD; In situ STM

## 1. Introduction

The process of underpotential deposition (UPD) of metals is known to be extremely sensitive to the surface structure of the electrode [1–7]. Among various UPD metals, Bi [7–10], Pb [7–9, 11–15] and Tl [7, 9, 14–16] have been studied extensively because Au electrodes with fractional coverages of those metal adlayers were reported to be significantly more active than either bare or monolayer-covered Au surfaces for the reduction of H<sub>2</sub>O<sub>2</sub> and O<sub>2</sub> [7–13].

Several in situ techniques have been used to understand the relationship between the electrocatalytic activity and the structure of UPD adlayers: the adlayer structures of Pb [17–19], Bi [20–24] and Tl [25, 26] on Au(1 1 1), and Pb [27], Bi [28, 29] and Sb [30, 31] on Au(1 0 0) have been studied using in situ scanning tunneling microscopy (STM), atomic force microscopy (AFM) and surface X-ray scattering (SXS). The results obtained by those in situ techniques provided direct insight into the relationship between surface struc-

ture and electrocatalytic activity. Recently, Li and Gewirth examined the mechanism of the H<sub>2</sub>O<sub>2</sub> electroreduction on Bi-submonolayer-modified Au(1 1 1) surface using density function theory calculations [32]. They suggested that the O atoms in H<sub>2</sub>O<sub>2</sub> interact strongly with two Bi atoms, and that a cleavage of the O–O bond occurs depending on the distance between adjacent Bi adatoms on the Au(1 1 1) surface. As the distance between Bi adatoms decreases with increasing coverage, H<sub>2</sub>O<sub>2</sub> can be adsorbed on Bi without breakage of the O–O bond.

Among the three admetals, namely Bi, Pb and Tl, which enhance the H<sub>2</sub>O<sub>2</sub> reduction, Bi allows the reaction to start at the most positive potential. The adlayer structure of Bi on Au(1 1 1) in HClO<sub>4</sub> solution was determined by Gewirth and co-workers using in situ AFM [20], STM [21] and SXS [21]. It was reported that the Bi adlayer exists in two different structures, (2 × 2) and (p × √3), at positive and negative potentials, respectively [20, 21]. It was also reported that the H<sub>2</sub>O<sub>2</sub> reduction proceeds at the highest rate on the (2 × 2) adlayer [20, 24, 33]. The rate of H<sub>2</sub>O<sub>2</sub> reduction on Bi-deposited Au(1 0 0) has been determined by Sayed and Jüttner [10]. Recently, we investigated the underpotential

\* Corresponding author. Tel.: +81 22 795 5868; fax: +81 22 795 5868.  
E-mail address: [itaya@atom.che.tohoku.ac.jp](mailto:itaya@atom.che.tohoku.ac.jp) (K. Itaya).

deposition process of Bi on Au(1 0 0) by in situ STM in detail [28,29]. However, to our knowledge, the structure of the UPD adlayer of Bi on Au(1 1 0) has not been determined.

In this paper, we report on underpotentially deposited Bi on Au(1 1 0) in HClO<sub>4</sub> investigated by using in situ STM at various electrode potentials.

## 2. Experimental

Single-crystal electrodes of gold were prepared by the method of Clavilier et al. [34] Briefly, a pure Au wire (0.7 mm in diameter) was melted in a hydrogen flame to form a single-crystal bead. A well-prepared single-crystal bead showed eight facets of (1 1 1) in an octahedral configuration and six facets of (1 0 0) in a hexahedral configuration. These facets usually exhibited a wide, atomically flat terrace-step structure. A (1 1 0) surface was mechanically exposed and polished with successively finer grades of Al<sub>2</sub>O<sub>3</sub> powder, from 1 to 0.3 μm in diameter. The final treatment, performed to expose a clean and ordered surface, consisted of flame annealing, slow cooling in a stream of hydrogen gas, and immersion in ultrapure water. The Au electrode was then transferred into the STM or the electrochemical cell with a drop of water protecting the surface from contamination.

In situ STM imaging was performed with Nanoscope E (Digital Instruments, Santa Barbara, CA). The STM tip was made from a W wire (0.25 mm in diameter) electrochemically etched in 1 M KOH. The tip was then coated with transparent nail polish to minimize the faradaic current. All STM images were acquired in the constant-current mode.

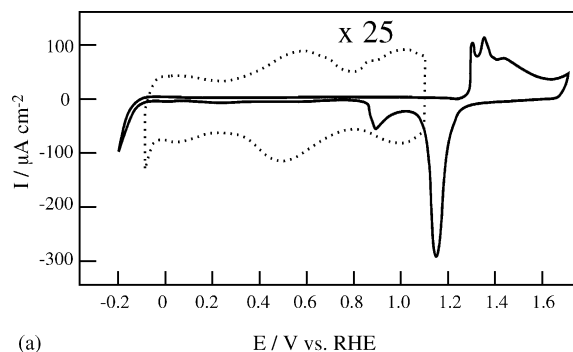
All electrolyte solutions were prepared with ultrapure HClO<sub>4</sub> (Cica-Merck), 99.9% Bi<sub>2</sub>O<sub>3</sub> (Wako Pure Chemical Industries, Ltd.), and ultrapure water (Millipore-Q). Electrode potentials are reported with respect to a reversible hydrogen electrode (RHE) in 0.1 M HClO<sub>4</sub>.

## 3. Results and discussion

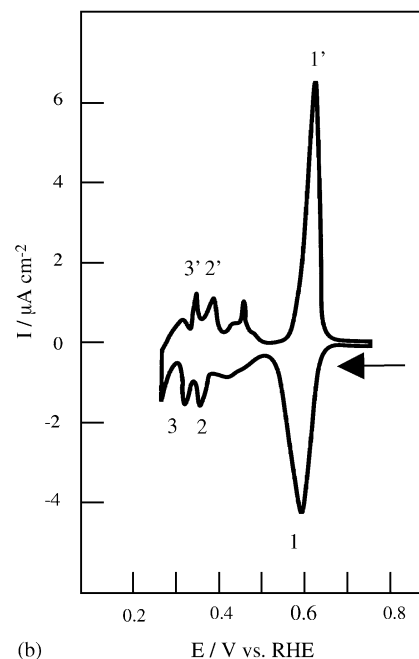
### 3.1. Cyclic voltammetry

A cyclic voltammogram (CV) of a well-defined Au(1 1 0) electrode in 0.1 M HClO<sub>4</sub> recorded at the scan rate of 50 mV s<sup>-1</sup> is shown in Fig. 1(a). The expanded-scale voltammogram obtained in the double-layer potential region (dotted line) and the two characteristic anodic peaks at 1.30 and 1.35 V (solid line) resulting from the oxidation of Au indicate that a well-defined Au(1 1 0) surface was exposed to the solution as described in the previous papers [35,36].

Fig. 1(b) shows a CV of Au(1 1 0) in 50 μM Bi<sub>2</sub>O<sub>3</sub> + 0.1 M HClO<sub>4</sub>. The electrode potential was initially scanned from 0.8 V in the negative direction at the scan rate of 2 mV s<sup>-1</sup>. The increase in cathodic current at 0.65 V is due to the first UPD of Bi. Peak 1 for the first UPD of Bi is seen at 0.6 V. Peak



(a)



(b)

Fig. 1. (a) Cyclic voltammogram of Au(1 1 0) electrode in 0.1 M HClO<sub>4</sub>; scan rate, 50 mV s<sup>-1</sup>. (b) Cyclic voltammogram of Au(1 1 0) electrode in 50 μM Bi<sub>2</sub>O<sub>3</sub> + 0.1 M HClO<sub>4</sub>; scan rate, 2 mV s<sup>-1</sup>.

2 at 0.35 V and Peak 3 at 0.3 V are associated with the second and the third UPD of Bi on Au(1 1 0) surface, respectively. The cathodic current commencing at 0.23 V is due to the bulk deposition of Bi. The peaks observed in the positive scan correspond to the dissolution of bulk Bi at 0.28 V and the successive dissolution of the three UPD layers (Peaks 3', 2' and 1'). The shape of the CV indicates that the UPD of Bi on Au(1 1 0) occurred in three steps. The pair of small cathodic and anodic peaks at the potential slightly positive to 0.43 V for Peaks 2 and 2' may be attributable to the UPD of Bi and its dissolution at a small portion of surface defects, such as steps and kinks [10]. The charges consumed during the UPD of Bi at Peaks 1, 2 and 3 were calculated to be approximately 270, 80 and 30 μC cm<sup>-2</sup>, respectively. The theoretical total charge corresponding to the deposition of a complete (1 × 1) monolayer of Bi on Au(1 1 0) is 410 μC cm<sup>-2</sup>, assuming that Bi<sup>3+</sup> in solution is transformed into Bi<sup>0</sup> upon adsorption on Au(1 1 0). By using the above values, the surface coverages of

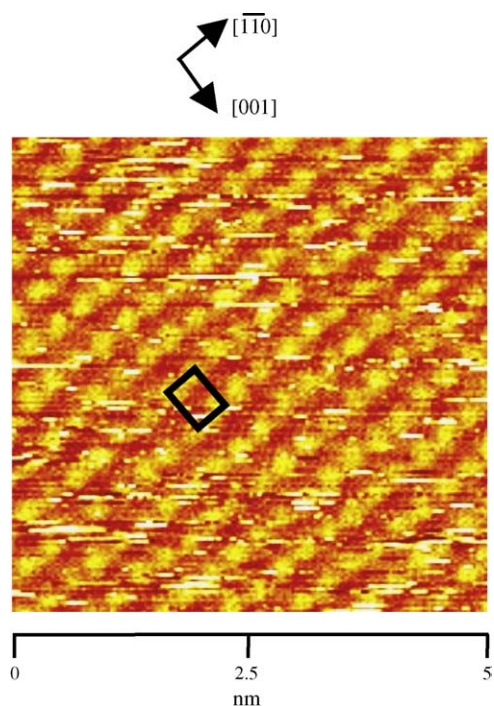


Fig. 2. STM top view of Au(110) surface in 0.1 M HClO<sub>4</sub>; scan area, 5 nm × 5 nm; electrode potential, 0.75 V; tip potential, 0.4 V; tunneling current, 20 nA.

Bi after the first, second and third UPD peaks were estimated to be 0.7, 0.8 and 0.9, respectively.

### 3.2. In situ STM measurement

STM measurements of Au(110) surface were first carried out in a pure 0.1 M HClO<sub>4</sub> solution before investigating the UPD. Fig. 2 shows a high-resolution STM image of Au(110) surface obtained at 0.75 V. The bright spots are seen to form a rectangular structure. The average distances between the spots, which are aligned in the  $[1\bar{1}0]$  and  $[001]$  directions, are approximately 0.29 and 0.42 nm, respectively. These lengths are identical to the Au–Au distances on Au(110), suggesting that each bright spot represents an Au atom, and that there is no reconstruction visible in the STM image of the Au(110) surface at 0.75 V. After the well-defined structure was observed on the well-prepared Au(110) surface in pure HClO<sub>4</sub>, the solution was replaced by 50 μM Bi<sub>2</sub>O<sub>3</sub> + 0.1 M HClO<sub>4</sub>. Then, STM images were obtained at 0.75 V, a potential more anodic than that for the first UPD (Fig. 1(b)). The well-ordered (1 × 1) structure was also observed on the Au(110) surface, indicating that Bi<sup>3+</sup> ions were not adsorbed on Au(110) surface in the potential region more anodic than that for the UPD.

Subsequently, the potential was stepped to a value more cathodic than that for the first UPD. Fig. 3(a) shows an STM image acquired at 0.5 V, a potential between Peaks 1 and 2 (Fig. 1(b)). Atomically flat terraces are extended with kinked winding steps of a monatomic height. The steps were sta-

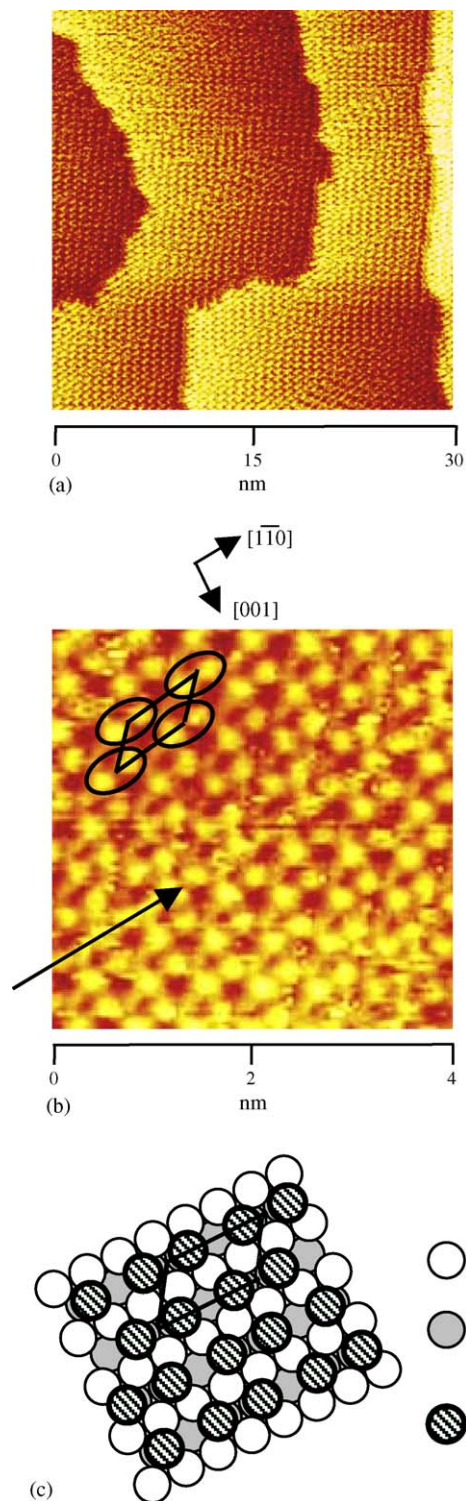


Fig. 3. (a) STM top view recorded at a potential after the first UPD peak of Bi on Au(110) in 50 μM Bi<sub>2</sub>O<sub>3</sub> + 0.1 M HClO<sub>4</sub>; scan area, 30 nm × 30 nm; electrode potential, 0.5 V; tip potential, 0.45 V; tunneling current, 20 nA. (b) High-resolution STM image of a Bi adlayer on Au(110) in 50 μM Bi<sub>2</sub>O<sub>3</sub> + 0.1 M HClO<sub>4</sub>; scan area, 4 nm × 4 nm; electrode potential, 0.5 V; tip potential, 0.35 V; tunneling current, 15 nA. (c) Structural model for the Bi adlayer deposited on Au(110) with a  $\begin{pmatrix} 3 & 0 \\ 1 & 1 \end{pmatrix}$  unit cell.

bly observed without changing their shapes. On the terraces, bright spots are seen to form an ordered structure with the same brightness. The rows of bright spots are aligned in the  $[1\bar{1}0]$  direction. A close-look at the image in Fig. 3(a) reveals that each spot is not circular but elongated in the  $[1\bar{1}0]$  direction of the rows of spots. A high-resolution STM image is shown in Fig. 3(b). The arrow in the middle of the image indicates a phase boundary running in the  $[1\bar{1}0]$  direction. The Au(110) surface is covered with small spots. Detailed examination of the STM image in Fig. 3(b) revealed that the small spots are arranged in pairs on the surface as encircled by ellipses; each elongated spot in Fig. 3(a) consists of a pair of small spots as seen in Fig. 3(b). The average atomic distance between the two spots which appear to form a dimer is approximately  $0.34 \pm 0.05$  nm. This distance is similar to that between two adjacent Bi atoms in a Bi single crystal, 0.32 nm, suggesting that each bright spot corresponds to a deposited Bi atom. A unit cell is outlined in Fig. 3(b) by solid lines with four Bi dimers at the corners. The longer sides of the unit cell are in the  $[1\bar{1}0]$  direction, whereas the shorter sides are tilted by  $42 \pm 5^\circ$  with respect to  $[1\bar{1}0]$ . The average length of the longer sides of a unit cell is  $0.85 \pm 0.07$  nm, whereas that of the shorter sides of a unit cell is  $0.52 \pm 0.05$  nm. Because the brightness is the same for all Bi atoms, they are thought to be situated at the same adsorption sites. The results described above indicate that the Bi adlayer on Au(110) formed at

0.5 V is of a  $\begin{pmatrix} 3 & 0 \\ 1 & 1 \end{pmatrix}$  structure, whose model is depicted in

Fig. 3(c). Based on the brightness of Bi atoms and the distance between them, each Bi atom is assigned to a near four-fold site. In this model, the lengths of the longer and shorter sides of the unit cell are 0.87 and 0.51 nm, respectively, which match the measured distances of 0.85 and 0.52 nm. However, the angle between the longer and shorter sides of a unit cell in the model is  $58^\circ$ , whereas the measured angle was  $42^\circ$ . We think that this difference is probably caused by the thermal drift. The coverage of Bi calculated from this structure is 0.66, which agrees well with the value obtained by the charge density measurement, 0.7, as described in the preceding section.

The electrode potential was then stepped to 0.35 V, which is a potential of Peak 2 (Fig. 1(b)). Fig. 4 shows an STM image. Bright spots aligned in the  $[1\bar{1}0]$  and  $[001]$  directions are seen to form an ordered rectangular structure on the atomically flat terraces. Interestingly, the step lines were obscure and mobile at this potential. A unit cell is shown in Fig. 4. The average atomic distances between the bright spots that form a unit cell are 0.29 and 0.41 nm, respectively. This unit cell of Bi adlayer is the same as that of the underlying Au(110)– $(1 \times 1)$  lattice. This  $(1 \times 1)$  structure was observed in the potential range for Peak 2 (Fig. 1(b)).

The structural change between  $\begin{pmatrix} 3 & 0 \\ 1 & 1 \end{pmatrix}$  and  $(1 \times 1)$ , which occurred when the electrode potential was changed, was reversible.

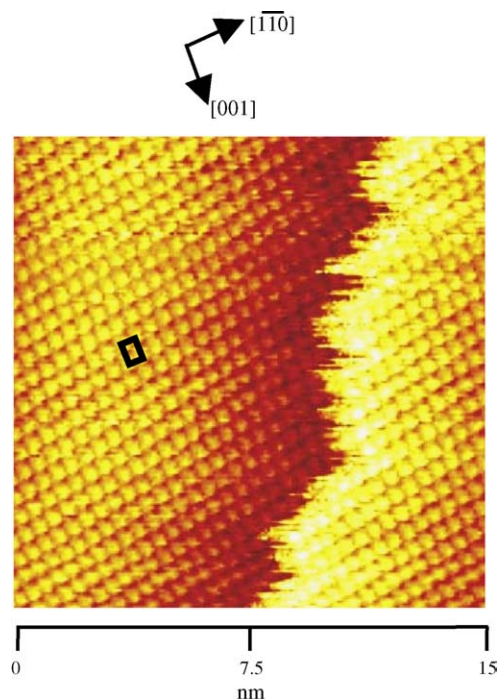


Fig. 4. STM top view recorded at a potential of the cathodic peak on Au(110) in  $50 \mu\text{M Bi}_2\text{O}_3 + 0.1 \text{ M HClO}_4$ ; scan area,  $15 \text{ nm} \times 15 \text{ nm}$ ; electrode potential, 0.35 V; tip potential, 0.45 V; tunneling current, 20 nA.

The coverage of Bi calculated from the  $(1 \times 1)$  structure should be equal to unity. However, this value is larger than the coverage of 0.8 obtained from the total charge density for Peaks 1 and 2 in the CV. Actually, because the shortest distance of Bi atoms in a crystal, 0.32 nm, is much larger than that of Au atom, 0.289 nm, the  $(1 \times 1)$  structure observed by STM would appear to be too dense for Bi atoms on Au(110). The difference between the coverage values obtained from CV (Fig. 1(b)) and from STM (Fig. 4) and the larger size of Bi atom, appears to suggest that the bright spots in the STM image in Fig. 4 might not represent Bi atoms but the substrate Au atoms.

The appearance of a  $(1 \times 1)$  structure of the Au substrate at a higher coverage observed in this study does not seem to be a usual case. For example, the disorder–order phase transition in an adsorbed sulfate layer is known to occur on Au(111) and Pd(111) surfaces in  $0.1 \text{ M H}_2\text{SO}_4$ . In the potential region of the disordered phase, an ideal  $(111)$ – $(1 \times 1)$  structure has been observed by STM even sulfate ions are adsorbed on the surfaces [37,38]. The same behavior was reported for Br- and Cl-adsorbed Au(100) surfaces [39]. However, in those cases, the  $(1 \times 1)$  structure has been observed only at low coverages of the adsorbates. On the other hand, it is important to point out again that the step lines were mobile at the potential for Peak 2. It has been reported that the presence of a strongly adsorbed layer suppresses the diffusion of Au atoms [28,31,39]. By comparing the mobility of Au atoms at step edges at a higher coverage of Bi (Fig. 4) with the stability

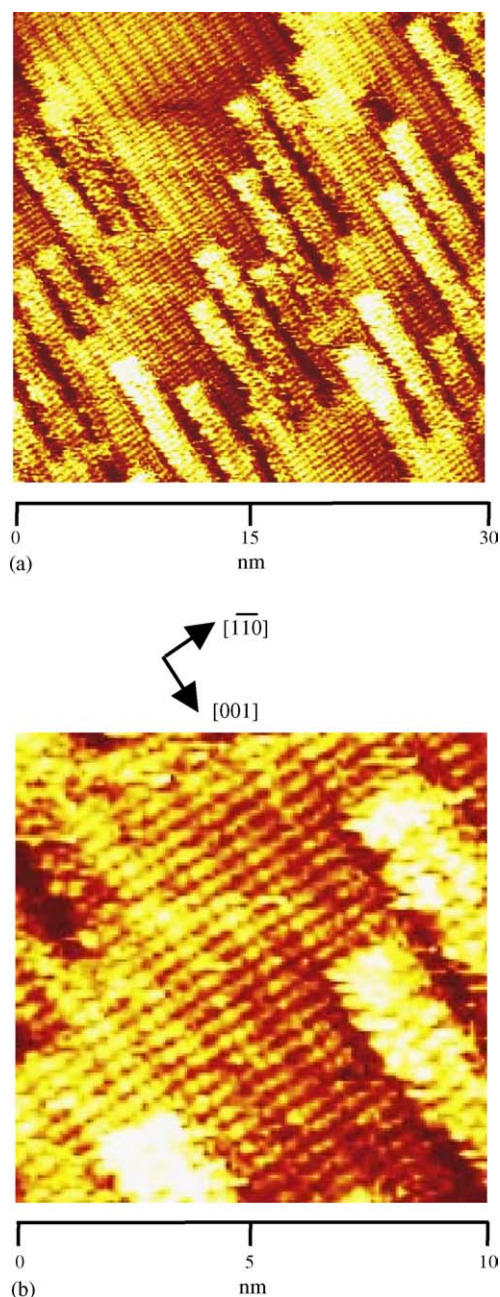


Fig. 5. (a) STM top view of Bi on Au(1 1 0) in 50  $\mu\text{M}$   $\text{Bi}_2\text{O}_3$  + 0.1 M  $\text{HClO}_4$ ; scan area, 30 nm  $\times$  30 nm; electrode potential, 0.27 V; tip potential, 0.35 V; tunneling current, 15 nA. (b) High-resolution STM image of Bi adlayer on Au(1 1 0) in 50  $\mu\text{M}$   $\text{Bi}_2\text{O}_3$  + 0.1 M  $\text{HClO}_4$ ; scan area, 10 nm  $\times$  10 nm; electrode potential, 0.3 V; tip potential, 0.35 V; tunneling current, 15 nA.

at a lower coverage (Fig. 3(a)), there seems to be a possibility that Bi atoms are only weakly adsorbed at Peak 2, forming a disordered phase on Au(1 1 0) surface.

The potential was then stepped to 0.27 V, which was in the potential range where the formation of the third UPD layer was completed. In the first minute after stepping the potential, the initially winding steps became straight, and rod-like arrays began to grow in the [0 0 1] or [0 0  $\bar{1}$ ] direction from

the step lines. Fig. 5 shows STM images acquired at 0.3 V 15 min after the potential step. The large-scale STM image in Fig. 5(a) shows that the rod-like arrays with a monoatomic height now run parallel to the [0 0 1] direction, or the direction of the atomic rows of the underlying Au(1 1 0) lattice. The width of the arrays is  $1.8 \pm 0.2$  nm, approximately six times the Au–Au distance in the [1  $\bar{1}$  0] direction. Weaver and co-workers found an adsorbate-induced substrate restructuring on Br- and I-adsorbed Au(1 1 0) surfaces [40–42]. They observed the erosion of terrace edges especially in the [0 0 1] direction and the appearance of arrays of single atomic layers of ‘nanorods’, 1.8 nm in width oriented in [0 0 1] on Br-adsorbed Au(1 1 0) [40]. The rod-like steps might have been formed on the Bi-adsorbed Au(1 1 0) surface to compensate for the surface tension and to lower the total surface energy [40]. Furthermore, a close examination of STM images revealed the presence of stripes of Bi on the terraces. Fig. 5(b) shows a high-resolution STM image, in which stripes of Bi are seen. The distance between stripes on the terrace is approximately  $1.2 \pm 0.1$  nm. In this image, the bright spots form a quadrilateral structure. The rows of the bright spots are along the atomic rows of the underlying Au(1 1 0) lattice, in the [1  $\bar{1}$  0] and [0 0 1] directions. Those Bi atoms exhibit different corrugation heights probably because Bi atoms are situated at different adsorption sites. The average atomic distances between the Bi atoms aligned in the [0 0 1] direction is  $0.41 \pm 0.05$  nm, which is equal to the Au–Au distance of Au(1 1 0) surface. On the other hand, the average atomic distance between Bi atoms aligned in the direction is  $0.38 \pm 0.05$  nm, which is greater than that of Au(1 1 0) surface, 0.289 nm. The striped structures must be caused by the mismatch between the adlattice of Bi and the substrate lattice of Au(1 1 0) [1,21,43]. The result described above indicates that Bi atoms formed an incommensurate adlayer at 0.3 V.

The stripe pattern was observed in the potential range for the third UPD peak (Fig. 1(b)). All UPD processes observed in this study were completely reversible with respect to the electrode potential. No alloy formation was indicated as in the case on Au(1 1 1) and (1 0 0) [20,21,28,29].

#### 4. Conclusions

The UPD process of Bi on Au(1 1 0) in  $\text{HClO}_4$  solution was investigated by electrochemical measurements and in situ STM. The UPD of Bi occurred in three steps. High-resolution STM images revealed that the Bi adlayer formed after the first UPD peak has a  $\begin{pmatrix} 3 & 0 \\ 1 & 1 \end{pmatrix}$  structure. STM images acquired at the second UPD peak showed a (1  $\times$  1) structure of Au(1 1 0). After the third UPD peak, the adsorbed Bi atoms formed stripes, and they were incommensurate with respect to the Au(1 1 0) substrate. All UPD processes observed in this study were reversible.

## Acknowledgments

This work was supported partially by the COE project, “Giant Molecules and Complex Systems, 2004”, from the Ministry of Education, Culture, Sports, Science and Technology, Japan, and by Core Research for Evolutional Science and Technology organized by the Japan Science and Technology Agency. The authors thank Dr. Y. Okinaka for his help in writing this manuscript.

## References

- [1] K. Itaya, *Prog. Surf. Sci.* 58 (1998) 121.
- [2] A.A. Gewirth, B.K. Niece, *Chem. Rev.* 97 (1997) 1129.
- [3] B.E. Conway, *Prog. Surf. Sci.* 16 (1984) 1.
- [4] A.T. Hubbard, *Chem. Rev.* 88 (1988) 633.
- [5] M.P. Soriaga, *Prog. Surf. Sci.* 39 (1992) 325.
- [6] J. Clavilier, A. Rodes, El. K. Achi, M.A. Zamakhchari, *J. Chim. Phys. Phys. Chim. Biol.* 88 (1991) 1291.
- [7] G. Kokkindis, *J. Electroanal. Chem.* 201 (1986) 217.
- [8] K. Jüttner, *Electrochim. Acta* 29 (1984) 1597.
- [9] K. Jüttner, *Electrochim. Acta* 31 (1986) 917.
- [10] S.M. Sayed, K. Jüttner, *Electrochim. Acta* 28 (1983) 1635.
- [11] M. Alvarez-Rizatti, K. Jüttner, *J. Electroanal. Chem.* 144 (1983) 351.
- [12] R.R. Adzic, A.V. Tripkovic, N.M. Markovic, *J. Electroanal. Chem.* 114 (1980) 37.
- [13] R. Adzic, A. Tripkovic, R. Atanasoski, *J. Electroanal. Chem.* 94 (1978) 231.
- [14] G. Kokkinidis, D. Sazou, *J. Electroanal. Chem.* 199 (1986) 165.
- [15] R. Amadelli, J. Molla, P. Bindra, E. Yeager, *J. Electrochem. Soc.* 128 (1981) 2706.
- [16] R. Amadelli, N. Markovic, R. Adzic, E. Yeager, *J. Electroanal. Chem.* 159 (1983) 391.
- [17] M.P. Green, K.J. Hanson, R. Carr, I. Lindau, *J. Electrochem. Soc.* 137 (1990) 3493.
- [18] M.P. Green, K.J. Hanson, *Surf. Sci. Lett.* 259 (1991) 743.
- [19] N.J. Tao, J. Pan, Y. Li, P.I. Oden, J.A. DeRose, S.M. Lindsay, *Surf. Sci. Lett.* 271 (1992) L338.
- [20] C.-H. Chen, A.A. Gewirth, *J. Am. Chem. Soc.* 114 (1992) 5439.
- [21] C.-H. Chen, K.D. Kepler, A.A. Gewirth, B.M. Ocko, J. Wang, *J. Phys. Chem.* 97 (1993) 7290.
- [22] I. Oh, M.E. Biggin, A.A. Gewirth, *Langmuir* 16 (2000) 1397.
- [23] T. Solomun, W. Kautek, *Electrochim. Acta* 47 (2001) 679.
- [24] K. Tamura, B.M. Ocko, J.X. Wang, R.R. Adzic, *J. Phys. Chem. B* 106 (2002) 3896.
- [25] W. Polewska, J.X. Wang, B.M. Ocko, R.R. Adzic, *J. Electroanal. Chem.* 376 (1994) 41.
- [26] R.R. Adzic, J.X. Wang, B.M. Ocko, *Electrochim. Acta* 40 (1995) 83.
- [27] U. Schmidt, S. Vinzelberg, G. Staikov, *Surf. Sci.* 348 (1996) 261.
- [28] M. Hara, Y. Nagahara, S. Yoshimoto, J. Inukai, K. Itaya, *J. Electrochem. Soc.* 151 (2004) 92.
- [29] M. Hara, Y. Nagahara, S. Yoshimoto, J. Inukai, K. Itaya, *Jpn. J. Appl. Phys.* 43 (2004) 7232.
- [30] J.W. Yan, Q. Wu, W.H. Shang, B.W. Mao, *Electrochem. Comm.* 6 (2004) 843.
- [31] M. Hara, J. Inukai, S. Yoshimoto, K. Itaya, *J. Phys. Chem. B* 108 (2004) 17441.
- [32] X. Li, A.A. Gewirth, *J. Am. Chem.* 125 (2003) 7086.
- [33] B.K. Niece, A.A. Gewirth, *Langmuir* 12 (1996) 4909.
- [34] J. Clavilier, R. Faure, G. Guinet, R. Durand, *J. Electroanal. Chem.* 107 (1980) 205.
- [35] A. Hamelin, *J. Electroanal. Chem.* 407 (1996) 1.
- [36] A.S. Dakkouri, D.M. Kolb, in: A. Wieckowski (Ed.), *Interfacial Electrochemistry*, Marcel Dekker Inc., New York, 1999, p. 151.
- [37] L.-J. Wan, T. Suzuki, K. Sashikata, J. Okada, J. Inukai, K. Itaya, *J. Electroanal. Chem.* 484 (2000) 189.
- [38] O.M. Magnussen, J. Hagebock, J. Hotlos, R.J. Behm, *Faraday Discuss.* 94 (1992) 329.
- [39] A. Cuesta, D.M. Kolb, *Surf. Sci.* 465 (2000) 310.
- [40] S. Zou, X. Gao, M.J. Weaver, *Surf. Sci.* 452 (2000) 44.
- [41] X. Gao, M.J. Weaver, *Phys. Rev. Lett.* 73 (1994) 846.
- [42] X. Gao, G.J. Edens, M.J. Weaver, *J. Phys. Chem. B* 98 (1994) 8074.
- [43] T. Yamada, N. Batina, K. Itaya, *J. Phys. Chem.* 99 (1995) 8817.